Comparative Analyses of Magnetic Field Correlation Imaging, Quantitative Susceptibility Mapping and Transverse Relaxation Rate R2* Indices of Brain Iron in Healthy Adults

Vitria Adisetiyo[1], Jens H. Jensen[1], Chu-Yu Lee[1], Donna R. Roberts[1], Maria V. Spampinato[1], and Joseph A. Helpern[1,2]

[1]*Radiology and Radiological Science, Center for Biomedical Imaging, Medical University of South Carolina, Charleston, SC, United States,* [2]*Neuroscience, Medical University of South Carolina, Charleston, SC, United States*

Target Audience: Scientists and clinicians interested in the application of magnetic resonance imaging indices of brain iron.

Purpose: Brain iron is required for important neurodevelopmental and functional processes (e.g., metabolism of neurotransmitters & myelin) and has been implicated in numerous neuropathologies [1-3]. The study of iron-related pathologies may, therefore, benefit from in vivo brain iron imaging methods. Brain iron is detected *non-invasively* with magnetic resonance imaging (MRI) mainly via the effect of magnetic field inhomogeneities (MFIs) and changes in magnetic susceptibility generated by non-heme iron on the MR signal [4]. Although conventional proton transverse relaxation rates (R2, R2* & R2′) are sensitive to detecting MFIs, their reduced specificity and reliability have been well documented [4]. Several advanced methods have been developed to overcome the limitations of relaxation rates, including magnetic field correlation (MFC) imaging and quantitative susceptibility mapping (QSM). Whereas MFC has a more direct relationship to MFIs than relaxation rates, in part because it is independent of dipolar relaxation mechanisms [5,6], QSM uses phase information to measure the inherent magnetic susceptibility in tissue [7,8]. The purpose of this study is to compare the application of MFC, QSM and R2* for assessing age-related brain iron changes in healthy adults and compare these results to putative postmortem non-heme iron concentrations in healthy brain [9]. The globus pallidus (GP), caudate nucleus (CN), putamen (PUT) and thalamus (THL) were chosen as regions of interest (ROI) because they have comparatively high iron levels and are regions where MFC, QSM and R2* metrics are most reliable [2,4,9].

Methods: This IRB approved study consists of 14 healthy adult males recruited from our institution's medical center (mean age 33.5 ± 12.1 years; range 19.2-59.6 years) with no pre-existing medical conditions (i.e., neurological, psychiatric, head injury, cerebrovascular, diabetes, asthma) and no prescription medication history. MR images were screened by a board-certified neuroradiologist (D.R.R) and all were interpreted as normal. Imaging was conducted on a 3T MR system (Siemens Trio) with a 32 channel head coil. Imaging parameters are: MFC asymmetric spin echo images: TR/TE = 5550/40 ms, voxel = 1.7 mm³, slices = 40, averages = 4, flip angle = 90°, EPI factor = 33, bandwidth = 1346 Hz/pixel. Refocusing pulse time shifts of 0, -4 and -16 ms, acquisition time = 6 min, 40 sec. QSM gradient echo images: TR/18TEs = 55/3.60 - 45.00 ms, voxel = 0.9 × 0.9 × 2.0 mm³, slices = 64, no gaps, average = 1, flip angle = 15°, bandwidth = 240 Hz/pixel, FOV = 240 × 240 mm², matrix = 256 × 256, acquisition time = 6 min, 18 sec. T2* gradient echo images: TR/10TEs = 4380/4.92 - 49.20 ms, voxel = 1.7 × 1.7 × 1.5 mm³, slices = 82, average = 1, flip angle = 20°, bandwidth = 260 Hz/pixel, acquisition time = 5 min, 34 sec. MFC and T2* images: no gaps, FOV = 220 × 220 mm², matrix = 128 × 128. T1-weighted MPRAGE images: TR/TE = 1900/2.26 ms, matrix = 192 × 256 × 256, voxel = 1 mm³, acquisition time = 4 min, 26 sec. The MFC and R2* parametric maps were calculated with in-house software [3]; QSM parametric maps were calculated using the Morphology Enabled Dipole Inversion algorithm [10]. For each age, putative postmortem non-heme iron concentrations (C_{PM}) in healthy brain regions were derived from Hallgren and Sourander's equations and data [9]. For each subject, automatic segmentation of the MPRAGE was performed using Freesurfer (http://surfer.nmr.mgh.harvard.edu). All segmented ROIs and parametric maps were normalized with ART2 [11,12] to a standard brain template provided by MRIcron (http://www.sph.sc.edu/comd/roden/mricron). For each normalized ROI, a consensus mask for the region was generated representing only voxels with 100% overlap among all subjects. Anatomical accuracy was verified by visual inspection. This consensus ROI was applied to the normalized parametric maps to extract ROI means from each subject. Comparison of each MRI metric with C_{PM} and each other were conducted with nonparametric Spearman correlations.

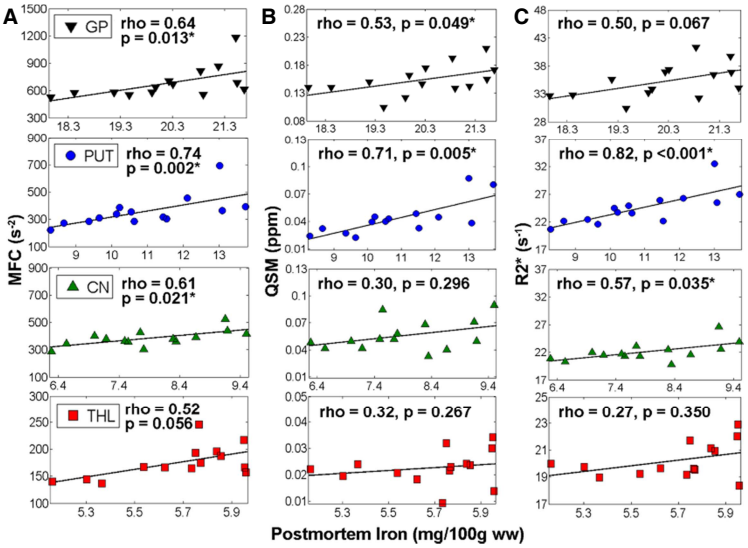

Figure 1. MFC, QSM & R2* correlations with Postmortem Iron (C_{PM})

Results: Combining all ROIs: C_{PM} significantly correlated with MFC (rho = 0.87), QSM (rho = 0.83) and R2* (rho = 0.92); all metrics significantly correlated with each other (MFC with QSM, rho = 0.92; MFC with R2*, rho = 0.88; QSM with R2*, rho = 0.87); all $p < 0.001$. Significant within ROI C_{PM} correlations with each metric: MFC in GP, PUT & CN (Figure 1A); QSM in GP & PUT (Figure 1B); R2* in PUT & CN (Figure 1C). Significant within ROI metric correlations: in GP, MFC with QSM (rho = 0.74) & R2* (rho = 0.90), QSM with R2* (rho = 0.84), all $p \leq 0.003$; in PUT, MFC with QSM (rho = 0.74) & R2* (rho = 0.86), QSM with R2* (rho = 0.88), all $p \leq 0.003$; in CN, MFC with R2* (rho = 0.87, $p < 0.001$), QSM with R2* (rho = 0.58, p = 0.030); in THL, QSM with R2* (rho = 0.74, p = 0.002).

Discussion and Conclusion: Our MFC, QSM and R2* values are consistent with the literature and, similar to previous reports, each metric significantly correlates with C_{PM} when assessing all regions together [2,13-16]. However, within regions, the metrics show differential correlations to C_{PM}. Whereas MFC significantly correlated to C_{PM} in GP, PUT & CN, QSM was significant only in GP & PUT and R2* in PUT & CN. These differences could stem from the distinct microscopic tissue properties of each region: neurons with short axons in PUT & CN; pervading nerve fiber bundles in GP & THL [17]. Indeed, all metrics may be altered by myelin, R2* is less accurate in regions of high iron concentration such as the GP, and QSM is affected by canceling phase shift effects from paramagnetic (e.g., iron) and diamagnetic substances (e.g., myelin, calcium) [2,4]. To our knowledge, this is the first study directly comparing MFC, QSM and R2*. Although significantly correlated with each other for our data, each metric provides different but complementary information about the variable characteristics of MFIs and magnetic susceptibility generated by regional non-heme tissue iron in brain. These distinctions may be useful in differentiating iron-related neuropathologies that affect specific regional iron properties (e.g., concentration, microscopic spatial distribution).

References: [1] Lozoff B. J. Nutr 141:740S-746S (2011). [2] Adisetiyo V, et al. JMRI 36:322-331 (2012). [3] Adisetiyo V, et al. Radiology 272:524-532 (2014). [4] Dusek P, et al. Int Rev Neurobiol. 110:195-239 (2013). [5] Jensen JH, et al. Magn Reson Med 55:1350-1361 (2006). [6] Jensen JH, et al. Magn Reson Med 61:481-485 (2009). [7] Schweser F, et al. Neuroimage 54:2789-2807 (2011). [8] Li W, et al. Neuroimage 55:1645-1656 (2011). [9] Hallgren B, Sourander PJ Neurochem 3:41-51 (1958). [10] Liu J, et al. Neuroimage 59:2560-2568 (2012). [11] Ardekani BA, et al. J Comput Assist Tomogr. 19:615-623 (1995). [12] Ardekani BA, et al. J Neurosci Methods 142:67-76 (2005). [13] Bilgic B, et al. Neuroimage 59:2625-2635 (2012). [14] Langkammer C, et al. Neuroimage 62:1593-1599 (2012). [15] Aquino D, et al. Radiology 252:165-172 (2009). [16] Langkammer C, et al. Radiology 257:455-462 (2010). [17] Piersol GA. Normal Histology 9th edition (1904).